AIAA-93-2978
Transition Effects on Compressible Dynamic Stall of Transiently Pitching Airfoils

M.C.Wilder, MCAT Institute, San Jose, CA;
M.S.Chandrasekhara, Naval Postgraduate School, Monterey, CA; and
L.W.Carr, U.S.Army ATCOM,
NASA Ames Research Center,
Moffett Field, CA

AIAA 24th
Fluid Dynamics Conference
July 6-9, 1993 / Orlando, FL

DISCLAIMER NOTICE

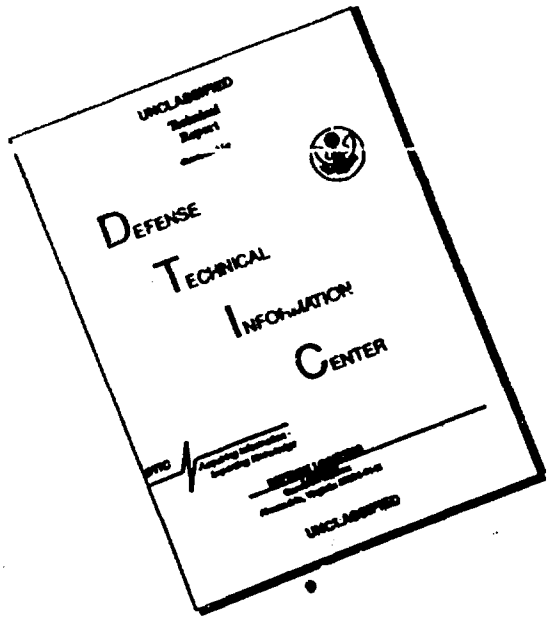

THIS DOCUMENT IS BEST QUALITY AVAILABLE. THE COPY FURNISHED TO DTIC CONTAINED A SIGNIFICANT NUMBER OF PAGES WHICH DO NOT REPRODUCE LEGIBLY.

Transition Effects on Compressible Dynamic Stall of Transiently Pitching Airfoils

M.C. Wilder[1]
Navy-NASA Joint Institute of Aeronautics and
MCAT Institute, San Jose, CA

M.S. Chandrasekhara[2,*]
Navy-NASA Joint Institute of Aeronautics
Department of Aeronautics and Astronautics
Naval Postgraduate School, Monterey, CA 93943

and
L.W. Carr[3]
U.S.Army ATCOM and Fluid Mechanics Laboratory Branch
NASA Ames Research Center, Moffett Field, CA 94035-1000

Abstract

Experimental results and analysis of the effects of boundary layer tripping on dynamic stall of a transiently pitching airfoil are presented. At low Mach numbers, the tripped airfoil exhibits qualitative similarity with the behavior of the untripped airfoil. However, the local supersonic flow at Mach numbers greater than 0.3 is significantly modified by the trip leading to vastly different shock/boundary layer interactions, dynamic stall onset and vortex formation angles. The formation of the laminar separation bubble is found to have a favorable influence in delaying dynamic stall on the untripped airfoil flow. In both Mach number regimes, the tripped flow actually stalls at slightly lower angles of attack. Further experimentation with three trips on an oscillating airfoil showed that the dynamic stall process is very sensitive to the state of the turbulence in the boundary layer. This sensitivity points to a need for finer turbulence modeling techniques for use in dynamic stall computations.

Nomenclature

C_p	pressure coefficient
c	airfoil chord
D_g	grit size
K	constant based on wind tunnel turbulence level
M	free stream Mach number
R	unit Reynolds number
Re	Reynolds number based on c and U_∞
U_∞	free stream velocity
x,y	chordwise and vertical distance
α	angle of attack
$\dot{\alpha}$	pitch rate in deg/sec
α^+	nondimensional pitch rate, $\frac{\dot{\alpha}c}{U_\infty}$

[1] *Research Scientist*

[2] *Associate Director and Research Associate Professor, Assoc. Fellow AIAA,*

***Mailing Address: M.S. 260-1, NASA Ames Research Center, Moffett Field, CA 94035-1000**

[3] *Research Scientist and Group Leader, Unsteady Viscous Flows, Aeroflightdynamics Directorate, Member AIAA*

1. Introduction

Dynamic stall is a problem of great interest to aerodynamicists since it offers the potential for enhancing the maneuverability and agility of aircraft. This potential is significantly affected by the onset of compressibility effects in flows over pitching airfoils. A sizeable data base[1,2] now confirms that above a free stream Mach number of 0.3, compressibility dominates the flow. Firstly, compressibility promotes premature stall. Additionally, the large flow acceleration can cause locally supersonic flows and induce a series of shocks[2,3] introducing other flow interactions. Available laboratory experiments on compressible dynamic stall have been conducted at low Reynolds numbers (300,000 to 1,000,000 - with the exception of McCroskey et al[4] and Lorber and Carta[5]). These low Reynolds number experiments have revealed that dynamic stall originates rapidly over a very small angle of attack range[3,6] as the laminar separation bubble that forms over the airfoil bursts. Further, most of the events of dynamic stall are concentrated near the leading edge region of the airfoil executing the rapid pitch-up motion. The formation of the separation bubble clearly indicates that the flow was laminar initially and then transitioned to reattach as a turbulent shear layer. Flow reattachment generally occurs[3] between x/c = 0.05 - 0.08 for the angle of attack range (6 -13 degrees) of interest in dynamic stall. The exact location depends upon where transition occurs and how the transition length is affected by the local flow conditions, in particular by the adverse pressure gradient. Gostelow et al[7] point out that the transition length is reduced considerably by large adverse pressure gradients. Thus, it should be expected that the transi-

tion process varies as the airfoil pitches up. Since low Reynolds number dynamic stall is intricately coupled to the bursting of the separation bubble, the process is also influenced by the transition process. To some extent, even high Reynolds number studies could be affected by this problem since the boundary layer is laminar near the stagnation point. Only when transition occurs before reaching the suction peak could one expect the bubble not to play a major role.

The experimental quantification of the role of transition on the details of the dynamic stall process is a daunting task. However, it is also an important task because the experimental data is needed for estimation of high Reynolds number behavior based on low Reynolds number experiments as well as, for computational code validation effort. It is worthwhile noting here that owing to the complex nature of the flow and a lack of the understanding of the physical processes, contemporary computational fluid dynamicists either ignore transition and perform a fully turbulent calculation[8] or arbitrarily fix[9] transition at a certain x/c location and invoke a turbulence model from this location in the computations. Thus, the usefulness of the computational results becomes severely limited for quantitative comparisons. Also, extrapolation of laboratory results to prototype or flight situations is also of limited value until this issue is addressed. In any case, validation of the computed data needs experimental results, which were hitherto not available.

The present paper reports some experimental results on compressible dynamic stall obtained by tripping the boundary layer with a three dimensional roughness. Most of the results will address the behavior of dynamic stall over a transiently pitching airfoil, which were obtained with a roughness height of about $175\mu m$. Subsequently, more measurements were performed to investigate the flow over an oscillating airfoil with this and two other roughness elements; these will be compared when appropriate. A real time point diffraction interferometry (PDI) technique was used to obtain the global as well as surface density fields. The images were processed to yield pressure distributions to compare the various cases quantitatively. The results clearly demonstrate the need for proper tripping of the boundary layer in these complicated flows.

2. Experimental Facility and Techniques

2.1. Facility Description

The results to be presented in this paper are part of an ongoing dynamic stall research program in the Navy-NASA Joint Institute of Aeronautics. The experiments were conducted in the *Compressible Dynamic Stall Facility (CDSF)* in the Fluid Mechanics Laboratory(FML) of NASA Ames Research Center. The facility permits study of dynamic stall over a range of Mach numbers, using non-intrusive optical flow diagnostic techniques. It is operated as a part of the in-draft tunnel complex at the FML (for details see Carr and Chandrasekhara[10]). In the CDSF, the airfoil is supported between two 2.54cm thick optical quality glass windows by pins. Since the pins are smaller than the local airfoil thickness, unobstructed optical access is available to the entire flow field. Thus it is possible to study the flow at the surface near the leading edge, where the dynamic stall vortex forms, as well as the flow field away from the airfoil.

The transient pitching motion was produced by a custom designed hydraulic system. Ref. 11 provides the details of the drive and these are briefly given below.

angle of attack, α:	0-60°
pitch rate, $\dot{\alpha}$:	0-3600 °/sec
maximum acceleration rate:	600,000 $°/sec^2$
change in α during acceleration:	$\leq 6°$ of pitch
minimum acceleration time:	4 ms
free stream Mach number:	0.1-0.5
airfoil chord:	7.62cm
Reynolds number:	$2x10^5$ - $9x10^5$

The angle of attack range and the highest pitch rate of 3600 °/sec on the 7.62 cm chord airfoil corresponds to a 90°/sec pitch rate of a 3m chord airplane wing at any given Mach number; thus, the rates obtainable from the design are directly applicable to flight conditions. The system controls are such that no effects of the system transients on flow separation are noticeable. The system uses both the airfoil position and velocity information in its feed back loops to properly execute any pre-programmed maneuver. The change in angle of attack during acceleration and the acceleration time itself are limited to less than 6° and 4 ms, respectively.

A digital optical encoder provided the instantaneous airfoil position. It was recorded from the digital I/O board of a microVAX II workstation and the pitch rate was timed with the computer internal clock. The pitch rate was constant to within 1% over the angle of attack range of interest at the highest pitch rates since it was specifically tuned for such rates. At slower rates, a mild change (less than 2%) was noticed at $\alpha = 15^0$. But, since this angle was considerably higher than the static stall or the dynamic stall onset angle, it is believed to have no effects on the results.

2.2. The Trip

Transition was fixed by applying a strip of randomly placed roughness elements along the upper surface of the airfoil, near the leading edge. A formula given in Ref. 13 was used to estimate the minimum size of the roughness elements required to trip the boundary layer. The formula is

$$D_g = \frac{12K}{R}$$

where D_g is the grit size in inches, R is the Reynolds number per foot of length for the free stream flow, and K is a constant which depends on tunnel turbulence level and may be assumed to be 400. This formula indicated a grit size diameter of $D_g = 56 - 89\mu m$ (0.0022 - 0.0035 in) for the Mach number range $0.2 \leq M \leq 0.3$.

Number 220 polishing grit with a size range of 74 - 89 μm (0.0029 - 0.0035 in) was selected for the construction of the boundary-layer trip. The grit was

glued to the airfoil surface with a water soluble adhesive (Polaroid print coating material). The region of airfoil surface around the intended trip location was masked off with tape, the glue was brushed on to the exposed surface, and then the grit was applied with an air brush to insure an even distribution of the roughness elements. The trip stretched the entire span of the airfoil and extended from x/c = 0.005 to x/c = 0.03 along the upper surface. A schematic is presented in Fig. 1 indicating the location and thickness of the trip. The profile was obtained from a digitized photograph of the airfoil under no-flow conditions and indicates that the maximum thickness of the trip was $175\mu m$. The added thickness was attributable to the adhesive base.

The results presented in this paper were obtained for a transiently pitching airfoil equipped with the trip described above. Subsequent experiments were performed on the flow over an oscillating airfoil with this and two other trips. The oscillating airfoil data are still being analyzed, but some preliminary results will be discussed where relevant. A spray-on enamel lacquer replaced the Polaroid coating as the bonding medium for the grit. The lacquer could be applied in a thiner coat and had a longer curing time, which facilitated applying the grit uniformly. The second trip was a thin version of the first trip with a maximum thickness of $\sim 100\mu m$, extending from x/c = 0.005 to x/c = 0.03. The third trip extended from x/c = 0.05 on the lower surface near the stagnation point and around the leading edge to x/c = 0.03 on the upper surface; the thickness was $\sim 130\mu m$.

2.3. Point Diffraction Interferometry Technique

The point diffraction interferometry technique used in this study utilized a point discontinuity (in the form of a pin-hole) located at the image of a point light source to diffract a portion of the incident light into a spherical reference wave front. In the present application, the primary optics of an existing schlieren system were used (see Ref. 12 for details), with a pulsed Nd:YAG laser replacing the conventional spark as the light source, and a specially created point diffractor replacing the usual knife edge. The laser light was expanded through a microscope objective to fill the schlieren mirror, transmitted through the test section, and refocused by another schlieren mirror. The exposed photographic plate used to create the point-diffraction spot was placed at the focus of this second mirror, and the laser was pulsed with enough energy to burn a hole, or spot, in the emulsion. The spot was created *in situ* by passing light through the test section at under no-flow condition. It was also precisely tailored to the application under investigation, automatically correcting for nonuniformities in the light source or optics. The tunnel was turned on and the real-time interference fringes were recorded on Polaroid film(ASA 3000), and were available for immediate viewing.

The analysis of the interferograms was conducted using a package developed in-house for the purpose. The PDI images were digitized and the images processed on an IRIS Work Station to obtain the fringe intersections with the airfoil contour. Using isentropic flow relations, the fringe numbers and hence, the fluid densities were converted to pressure coefficients. This assumption was made even through the boundary layer and the vortex, for lack of better flow relations. However, it is not believed to introduce substantial errors in the pressure field, since the entropy change is generally small, until deep stall occurs.

2.4. Experimental Conditions

The experiments were conducted on a 7.62 cm chord, NACA 0012 airfoil. The following conditions were chosen for the tripped airfoil studies. (The corresponding data for the untripped airfoil was already available[3]).

M	α^+					
	0	0.02	0.025	0.03	0.035	0.04
0.2	X		X	X		X
0.3	X	X	X	X	X	X
0.45	X	X	X	X		

The chord Reynolds number ranged from 360,000 at M = 0.2 to 810,000 at M = 0.45. The airfoil was pitched from 0 - 60^0 about the $\frac{1}{4}c$ point. The interferograms were obtained at the desired instantaneous angles of attack during separate pitch-up motions (one picture/pitch-up) for 0 - 20^0 angle of attack by strobing the laser externally. The laser pulse was $\approx$ 60 nanoseconds. There was no delay between the selected angle of attack and the angle of attack at which the laser pulse was actually seen, which was detected by a photodetector that latched the encoder display when the laser pulsed.

2.5. Experimental Uncertainties

The following are the estimated uncertainties in the various quantities:

Mach number:	± 0.005
angle of attack:	0.1 degrees
normalized pitch rate:	$\pm 0.5\%$ at rates $> 2000^0/sec$
	$\pm 1\%$ at rates $< 2000^0/sec$
C_p:	at M = 0.2, $\pm$ 0.225
	at M = 0.3, $\pm$ 0.075
	at M = 0.45, $\pm$ 0.0375
$\frac{dC_p}{d(x/c)}$	± 10

The uncertainty in C_p is estimated to be 1 fringe for the flow in general with about 3 fringes possibly undetectable for the peak suction pressure coefficient.

3. Results and Discussion

The pressure distributions derived from an analysis of the interferogram images will first be presented along with a qualitative discussion of representative images used as flow visualization. A discussion of the leading-edge pressure gradients calculated from the pressure distributions will follow. Comparisons will

be made between results obtained on an untripped and a tripped airfoil.

3.1. Interferogram Images and Pressure Distributions

Analysis of untripped airfoil[3] steady - and unsteady - flow[3] interferograms of the airfoil flow field while the airfoil rapidly pitches from 0 to 60 degrees angle of attack has shown that a leading-edge laminar separation bubble forms in both steady and unsteady flows for all Reynolds numbers of the experiment. Furthermore, for the low Mach numbers studied in the untripped case, the dynamic stall vortex originated just as the bubble burst; the vortex then grew and convected. Tripping the boundary layer ensured that the flow was turbulent from the origin of the trip, which means that a laminar separation bubble could not form. The result of tripping the boundary layer is illustrated in Fig. 2 for the conditions M = 0.3, $\alpha = 11^0$ and a nondimensional pitch rate of $\alpha^+ = 0.04$. Enlarged interferogram images of the leading-edge region for the untripped and tripped cases are presented in Figs. 2a and 2b, respectively. The instantaneous pressure coefficient distributions which were derived from these images are given in Fig. 2c. For both cases a peak suction pressure coefficient of $C_p = -3.4$ was measured, with the location of the suction peak in the tripped case shifted slightly downstream of the location of the peak in the untripped case (from x/c = 0.013 to x/c = 0.018). The laminar separation bubble appears in the untripped airfoil data as a plateau in the pressure coefficient plot which extends from $x/c \approx 0.025$ to $x/c \approx 0.055$.

The evolution of the dynamic stall vortex was greatly affected by the trip, as is illustrated in Fig. 3. Again for the conditions M = 0.3, $\alpha^+ = 0.04$, the earliest stage of dynamic stall vortex development began for the untripped airfoil as the airfoil passed instantaneously through the angle $\alpha = 15^0$, as can be seen in the interferogram shown in Fig. 3a. Here, the early stages of vortex development on the untripped airfoil is indicated by the opening of the separation bubble, which is made evident by the change in curvature of the fringes at the downstream end of the bubble (compared to Fig. 2a, where the fringes of the closed bubble meet the airfoil normal to the surface). In contrast, however, as the tripped airfoil passed this angle (Fig. 3b) the vortex had already grown considerably and covered the first 25% of the airfoil chord. The growth of the vortex can also be seen in the pressure coefficient distributions shown in Fig. 3c. As the vortex forms, the pressure coefficient distribution begins to 'lift' up along the suction surface, and as the vortex grows in extent and convects downstream, the increased region of suction along the upper surface results in the vortex lift of dynamic stall.

The development of the pressure coefficient distribution over the angle of attack range of $\alpha = 7^0$ to $\alpha = 17^0$ is shown in Fig. 4 for both the untripped and tripped airfoils for the conditions M = 0.3 and $\alpha^+ = 0.03$. The separation bubble, which began to develop at $\alpha \approx 9^0$ on the untripped airfoil (Fig. 4a), is clearly absent on the tripped airfoil (Fig. 4b). Further, for angles of 13 degrees and above (Fig. 4c and 4d) the untripped airfoil has developed a stronger suction, while the tripped airfoil stalled at approximately one degree lower angle of attack than the untripped airfoil (14^0 *vs* 15^0) as can be seen clearly by comparing Figs. 4c and 4d. In addition, the location of the suction peak moved slightly downstream for the tripped airfoil with increasing angle of attack, unlike that for the untripped case, where it moved towards the leading edge.

At higher subsonic free stream Mach numbers the leading-edge flow can become locally supersonic. In the case of the untripped airfoil it was shown[2,3] that multiple $\lambda-$shocks formed near the leading edge over the suction surface for freestream Mach numbers above $M \approx 0.4$. In contrast however, at most only two shocks were observed on the tripped airfoil at M = 0.45, indicating that forcing transition has dramatically altered the boundary layer/shock interaction physics. Interferograms of the untripped and tripped flows are shown in Fig. 5a and 5b, respectively, for the conditions of M = 0.45, $\alpha = 11^0$ and a nondimensional pitch rate of $\alpha^+ = 0.025$. A total of five shocks formed on the untripped airfoil for these conditions with the final shock occurring at nearly 10% of the chord from the leading edge. Only two shocks occurred in the tripped flow, with the final shock located near the downstream end of the trip at about the 3% chord point. Fringe counting showed that for the untripped flow, the local Mach number was supersonic until a height of about 2% chord above the airfoil surface, and the maximum Mach number was about 1.25. On the other hand, the supersonic region for the tripped airfoil extended to 1% chord above the airfoil and the Mach number was also lower at about 1.1. In both cases, the supersonic flow transitioned to the outer subsonic flow through a compression wave, through which the interference fringes were found to bend. The Mach number where this bending effect was masked was about 0.85. The location of the shocks in relation to the trip is illustrated more clearly in Fig. 5c, a composite of data obtained from digitized images of the trip and of the interferogram shown in Fig. 5b. The bold lines in this figure represent the supersonic flow and the dashed lines, the remainder of the compression waves.

Another striking feature seen in both the interferograms of Fig. 5 is the appearance of the vertical fringes following the last shock. In Ref. 3, this was shown to be associated with the first indication of the onset of dynamic stall. The studies reported in Ref. 3 also showed that even after the dynamic stall vortex formed (near the end of the bubble), the leading edge pressure coefficient remained large, until the influence of the vortex was felt near the leading edge. After this event, the pressure coefficient dropped rapidly as the vortex began to convect. In the higher Reynolds number experiments of McAlister et al[14], dynamic stall onset was said to correlate with the loss of the suction peak. However, the present interferometry studies seem to define stall onset more precisely. Fig. 5b shows the presence of the vertical fringes clearly and a slight reversed flow[3] is seen for $0.03 \leq x/c \leq 0.06$. Fringes pointing upstream in a thin layer of fluid below the separated shear layer are evidence of the locally reversed flow. This leads one to infer that that the dynamic stall process is under way - even though

there is a shock still present above the shear layer. On the other hand, although the vertical fringes are seen for the same experimental conditions of M = 0.45 and $\alpha = 11^0$ for the untripped flow, dynamic stall has just been initiated, since the region of reversed flow is still not easily discernible. Because the dynamic stall vortex originates at x/c $\approx$ 0.1, a definite delay exists between when the vortex forms (either because of the bursting of the laminar separation bubble or due to shock induced separation) and when its influence reaches the leading edge. During this time, the airfoil could continue to develop suction as the angle of attack is increased. This difference in the dynamic stall onset location between the two flows explains why the tripped airfoil flow stalls at a slightly lower angle of attack than when it is not tripped.

3.2. The Peak Suction Pressure

As mentioned earlier, the suction pressure reaches a maximum value just prior to dynamic stall onset; during the period while the dynamic stall vortex is growing, the suction remains high and then drops sharply once the vortex begins to convect. The peak suction pressure coefficient reached is shown in Fig. 6 for different nondimensional pitch rates and Mach numbers. Plotted for comparison on the same graph are the results obtained previously[3] for the untripped airfoil. In both cases, the peak suction pressure coefficient decreased dramatically with increasing Mach number, due to the increasing compressibility effects on the flow. This effect is seen in Fig. 6 for the tripped airfoil as a generally monotonic increase in the peak suction pressure coefficient with increasing nondimensional pitch rate. For the untripped airfoil, however, the peak suction pressure coefficient tended to be relatively independent of nondimensional pitch rate for $\alpha^+ > 0.03 (> 0.02$ for M = 0.45). This independence of the peak C_p on nondimensional pitch rate (for high pitch rates) in the untripped flow was presumably due to the presence of the separation bubble; the change in the shape of the enveloping streamline due to the presence of the bubble altered the inviscid/viscous interaction, and eventually limited the growth of the suction peak so that increasing the pitch rate further had no effect on the peak suction level reached.

The peak C_p tended to be less for the tripped airfoil than for the untripped airfoil for the same experimental parameters at Mach numbers $\geq$ 0.3. At the low Mach number of 0.2 the difference is represented by a single fringe in the interferograms; therefore, within the accuracy of the image analysis the peak C_p value was unaffected by the trip for this case. For the higher Mach number flows, where compressibility effects dominated, the difference was significant; five or more fringes for M = 0.3 which corresponded to $\Delta C_p > 0.81$, and four or more fringes for M = 0.45, or $\Delta C_p > 0.28$. The differences in the behavior seen for the different Mach numbers are typical of this flow since compressibility effects set in at M = 0.3[2].

3.3. The Adverse Pressure Gradient

The nondimensional adverse pressure gradient following the leading-edge suction peak was determined from the pressure coefficient distributions obtained from the analysis of the interferogram images by performing a linear least squares fit to the first three or four data points following the highest pressure coefficient value measured. As an example, Figs. 7a and 7b show the leading-edge instantaneous C_p distributions on the suction surface of the untripped and tripped airfoils, respectively, for the angles $\alpha = 12^0$, 13^0, and 13.5^0 at M = 0.3 and $\alpha^+ = 0.03$. Indicated on each curve is the straight line segment used to estimate the value of the pressure gradient $\frac{dC_p}{d(x/c)}$. No fit was performed for the $\alpha = 13.5^0$ data of the untripped case since only two fringes were detected in the adverse pressure gradient upstream of the separation bubble; often at higher angles no fringes are detectable in the suction peak. For the tripped airfoil flow (Fig. 7b), the dramatic change in the pressure distribution and the gradient which occurred between the angles $\alpha = 13^0$ and $\alpha = 13.5^0$ was a result of the formation and convection of the dynamic stall vortex.

The flattening of the distributions at the top must be commented on since, in general, the pressure coefficient distribution is a smooth and continuous function with a well defined peak. Inherent to the interferometry technique are in-plane deflections of the light rays due to the steep density gradients found at high angles of attack (for example at $\alpha = 12^0$) which have been shown to deflect the image of the beam into the airfoil surface[15], resulting in a reduction of the number of fringes visible. These 'missing fringes' cause the flat distribution and result in an under estimation of the value of C_p at the suction peak. It is also possible that the trip physically obscured some fringes very close to the surface.

The leading-edge adverse pressure gradients for the tripped and untripped airfoils are compared in Fig. 8a for the nondimensional pitch rate of $\alpha^+ = 0.03$, and M = 0.2. Also shown for comparison in Fig. 8b are the peak suction pressure coefficients for each angle of attack. Until the separation bubble formed (at $\alpha \approx 10^0$), the magnitude of the C_p gradient was similar for both the tripped and untripped airfoils. After the bubble formed the value of the gradient rose sharply in the untripped case. For both cases the gradient attained a maximum value about two degrees (of angle of attack) prior to the onset of dynamic stall and remained relatively constant until the onset of stall. As the dynamic stall vortex began to form, the magnitude of the gradient dropped sharply. This sudden drop in the magnitude of the adverse pressure gradient coincided with the initial development of the dynamic stall vortex and the appearance of the vertical fringes in the interferogram images. The drop occurred at $\alpha = 14^0$ for the tripped airfoil and $\alpha = 15^0$ for the untripped airfoil. Two degrees later the leading-edge suction pressure dropped in magnitude (Fig. 8b) and the dynamic stall vortex began to convect downstream.

This general trend, where the magnitude of the gradient stops growing approximately two degrees prior to the onset of stall and then drops sharply as the vortex begins to form, appears to be independent of both Mach number (Fig. 9) and nondimensional pitch rate (Fig. 10) until the local flow becomes supersonic. Figure 9 shows the pressure gradient as a

function of angle of attack for the Mach numbers M = 0.2, 0.3, and 0.45 and the nondimensional pitch rate of 0.03, while Fig. 10 shows the results for several pitch rates at M = 0.3. It is seen in these two figures that the magnitude of the adverse pressure gradient from which the flow can recover increases with increasing unsteadiness and decreases with increasing Mach number. This is consistent with the pitch rate and Mach number effects on the development of compressible dynamic stall which have been reported elsewhere[2,3]. The lack of data for the untripped airfoil at higher angles of attack for M $\geq$ 0.3 was a result of the PDI image distortions (i.e., the 'missing fringes') discussed earlier in this section. The character of the pressure gradient at M = 0.45 is of particular interest. Fig. 9a shows the untripped airfoil results, where the maximum $\frac{dC_p}{d(x/c)}$ experienced a *decrease* with angle of attack, at most, this $\frac{dC_p}{d(x/c)}$ remains constant for the tripped airfoil (Fig. 9b). This result clearly demonstrates the strong influence of compressibility on the flow development, reflecting the impact of the multiple shocks that have been observed at these conditions.

For all the parameters investigated, when the local flow remained subsonic, the untripped airfoil was found to be capable of withstanding a stronger adverse pressure gradient before dynamic stall onset than the tripped airfoil. Likewise, the peak suction pressure at stall was higher on the untripped airfoil than on the tripped airfoil (refer to Fig. 6). It appears that the formation of the separation bubble had a beneficial effect on stall for the conditions of the experiments. Evidence for this conclusion is based largely on the data shown in Fig. 8a, which clearly shows a similar development in the pressure gradient for both tripped and untripped flows at M = 0.2. Moreover, the appearance of the vertical fringes (which signify the onset of stall) coincides with the drop in the magnitude of the pressure gradient where data were available, and occurs two degrees before the drop in peak C_p (which occurs as the vortex convects downstream) for the cases studied. This would indicate that the mechanism of the dynamic stall vortex development was unaffected by the separation bubble at low Mach numbers. The picture is considerably different at higher Mach numbers as discussed in relation to Fig. 5.

3.4. Discussion of the Experimental Observations

The results presented in this paper briefly describe the first effort in assessing the role of transition on the compressibility effects on dynamic stall of pitching airfoils. It was originally presumed that use of a transition trip would render the local boundary layer turbulent and hence, a dramatically different sequence of events of dynamic stall would occur and improved stall characteristics for the airfoil would result. But, contrary to the expected results, a detailed analysis of the interferogram images revealed that the trip for which the data are presented actually caused dynamic stall at lower angles of attack than for the untripped airfoil.

It is to be noted that as shown in Fig. 8a at M = 0.2 and $\alpha^+ = 0.03$, the pressure gradient when the untripped flow first stalls and forms a bubble is about 100, whereas the pressure gradient for the tripped flow at first stall (which is dynamic stall) is about 200. These levels confirm what is expected of the ability of the tripped flow to withstand a larger adverse pressure gradient. In this context, the value of 350 for the pressure gradient at dynamic stall vortex formation for the untripped case seems apparently inconsistent. However, this may not be the case, since the untripped flow originally stalled at a pressure gradient of 100 forming the laminar bubble which changed the pressure distribution over the airfoil. Dynamic stall in this case arose out of the 'failure' of the laminar separation to reattach, thus bursting the bubble[3]. The local pressure gradient at the downstream edge of the bubble was also found to be about 100. Once the stall vortex formed, the gradient dropped sharply. It appears that after the bubble forms, the pressure gradient could still increase, because the separated shear layer could reattach until a certain higher angle of attack. The pressure gradient at stall decreases with increasing Mach number, but the above trend is still valid. At M = 0.45, the vortex forms at a very low value of $\frac{dC_p}{d(x/c)} = 25$ in the tripped flow. Data could not be processed in the untripped flow because of a larger region of the supersonic flow and the more complicated multiple shocks/compression waves interactions affecting the process.

Fig. 10a and 10b show that in steady flow, the tripped airfoil stalls at a lower angle of attack than the untripped airfoil. (Similar effects have been observed elsewhere, cf: the results for the NLR1 airfoil[14] where the tripped airfoil stall is 1 degree lower than the untripped airfoil stall angle) However, even for steady flow, the values of the adverse pressure gradient when the laminar separation bubble forms and when the tripped airfoil stalls are very close (70-100). One factor that could affect this number is the thickness of the trip used. As stated earlier, at 175μm, it was considerably more than the estimated boundary layer thickness of about 60 μm. The trip height was based on recommendations generally given for a flat plate boundary layer. The challenge of finding the 'right trip' for an unsteady flow with a large adverse pressure gradient, locally supersonic flow and in which the transition point moves considerably, is formidable. Further, standard recommendations on trip selection seem to be based on the fact that the boundary layer eventually reaches the equilibrium state. When leading edge separation occurs as in the present dynamic stall flow, this criterion is obviously not satisfied. Also, the stall process is significantly affected by the 'age' of the turbulence in the tripped boundary layer. If the turbulence is 'young' as in the present experiments, major differences could be found for each trip that is used. In fact, the experiments were repeated for an oscillating airfoil with three different trips. Preliminary evaluation of the data showed trends similar to those described in this paper, although the pitch angle was varied in a sinusoidal manner. Further analysis is on-going. A typical plot of C_p *vs.* α for these trips is shown in Fig. 11, in which changes in C_p near stall onset caused by the various trips are clear. This also brings out the extreme sensitivity of the dynamic

stall process to the local flow details. This conclusion will be of great significance in computational modeling of the flow, especially when selecting a turbulence model. Until the computational fluid dynamics models include these complex physical effects, it appears to be unreasonable to expect quantitative agreement between experiments and computations.

4. Concluding Remarks

A study of the role of boundary layer tripping on dynamic stall of a transiently pitching airfoil has been conducted. The following conclusions are drawn from the study.

1. The laminar separation bubble present in the untripped flow was found to have a beneficial effect on dynamic stall delay.

2. Dynamic stall onset moves closer to the leading edge in the presence of a trip, which eventually leads to stall at lower angles of attack (by about 1 - 1.5 degrees) than observed in untripped airfoil dynamic stall.

3. The leading-edge adverse pressure gradient and the peak suction pressure coefficient were lower in value on the tripped airfoil.

4. The behavior of the flow is grossly different under compressibility conditions with a trip. The shock/boundary layer interactions are modified by the trip, as also is the leading edge pressure gradient.

5. The sensitivity of the flow to the state of the boundary layer turbulence points to a need for highly refined computational flow modeling.

Acknowledgements

The project was supported by an AFOSR grant (MIPR-93-0003) to the Naval Postgraduate School and was monitored by Maj. D.B. Fant. Additional support was received by ARO-MIPR-125-93, monitored by Dr. T.L. Doligalski. The work was carried out in the Fluid Mechanics Laboratory Branch of NASA Ames Research Center. The steady encouragement of Dr. S.S. Davis, Chief, FML Branch, the support of Mr. J.D. Loomis in the conduct of experiments and the interferogram processing software development effort of Mr. P.J. Trosin, Sterling Federal Systems, Inc., are greatly appreciated.

5. References

[1]Chandrasekhara, M.S. and Carr, L.W., "Flow Visualization Studies of the Mach Number Effects on the Dynamic Stall of an Oscillating Airfoil", *Journal of Aircraft*, Vol. 27, No. 6, pp. 516-522.

[2]Chandrasekhara, M.S., Ahmed , S. and Carr, L.W., "Schlieren Studies of Compressibility Effects on Dynamic Stall of Airfoils in Transient Pitching Motion", *Journal of Aircraft*, Vol. 30, No. 2, pp. 213-220.

[3]Chandrasekhara, M.S. and Carr, L.W., and Wilder, M.C., "Interferometric Investigations of Compressible Dynamic Stall Over a Transiently Pitching Airfoil", *AIAA Paper 93-0211*, Accepted for publication in *AIAA Journal*

[4]McCroskey, W.J., McAlister, K.W., Carr, L.W., Pucci, S.L., Lambert, O., and Indergrand, R.F., "Dynamic Stall on Advanced Airfoil Sections", *Journal of American Helicopters Society*, Vol. 26, No. 3, pp. 40-50.

[5]Lorber, P.F. and Carta, F.O., "Unsteady Stall Penetration Experiments at High Reynolds Number", AFOSR-TR-87-1202, April 1987.

[6]Carr, L.W., Chandrasekhara, M.S., Ahmed, S., and Brock, N.J., "A Study of Dynamic Stall Using Real Time Interferometry", *AIAA Paper 91-0007*, Accepted for publication in *Journal of Aircraft.*

[7]Gostelow, J.P., Blunden, A.R., and Walker, G.J., "Effects of Free-Stream Turbulence and Adverse Pressure Gradients on Boundary Layer Transition", *ASME Paper No. 92-GT-380*, presented at the International gas Turbine and Aero Engine Congress and Exposition, Cologne, Germany, June 1-4, 1992.

[8]Visbal, M.R., "Effect of Compressibility on Dynamic Stall of a Pitching Airfoil", AIAA Paper No. 88-0132, Jan. 1988.

[9]Chandrasekhara, M.S., Carr, L.W., Ekaterinaris, J.A., and Platzer, M.F., "Interferometry and Computational Studies of an Oscillating Airfoil Compressible Dynamic Stall", Proceedings of *The 5th Asian Congress of Fluid Mechanics*, Vol. 2, pp. 1047-1050, Ed. K.S. Chang and D.H. Choi, Aug. 1992.

[10]Carr, L.W., and Chandrasekhara, M.S., "Design and Development of a Compressible Dynamic Stall Facility", *Journal of Aircraft*, Vol. 29, No. 3, pp. 314-318.

[11]Chandrasekhara M.S., and Carr, L.W., "Design and Development of a Facility for Compressible Dynamic Stall Studies of a Rapidly Pitching Airfoil", *ICIASF'89 RECORD*, IEEE Publication 89-CH2762-3, pp. 29-37.

[12]Brock, N.J., Chandrasekhara, M.S., and Carr, L.W., "A Real Time Interferometry System for Unsteady Flow Measurements", *ICIASF'91 RECORD*, IEEE Publication 91-CH3028-8, pp. 423-430.

[13]Pope, A., and Goin, K.L., *High Speed Wind Tunnel Testing*, Kraeger Publishing Company, New York, NY, 1978.

[14]McAlister, K.W, Pucci, S.L., McCroskey, W.J., and Carr, L.W., "An Experimental Study of Dynamic Stall of Advanced Airfoil Sections, Volume 2, Pressure and Force Data", NASA TM 84245, Sept. 1992.

[15]Cho, Y.C., Carr, L.W., and Chandrasekhara, M.S., "Correction to Fringe Distortion due to Flow Density Gradients in Optical Interferometry" *AIAA Paper No. 93-0631*, presented at the 31st Aerospace Sciences Meeting and Exhibit, Reno, NV, Jan, 11-14, 1993.

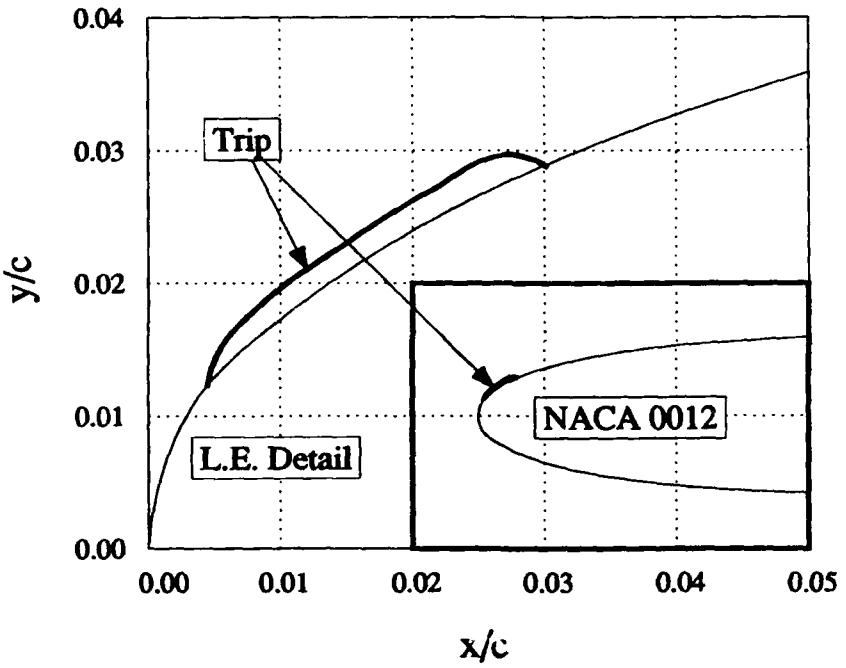

Figure 1. Profile View of the Boundary-Layer Trip. Inset Shows the Leading 25% of the Chord.

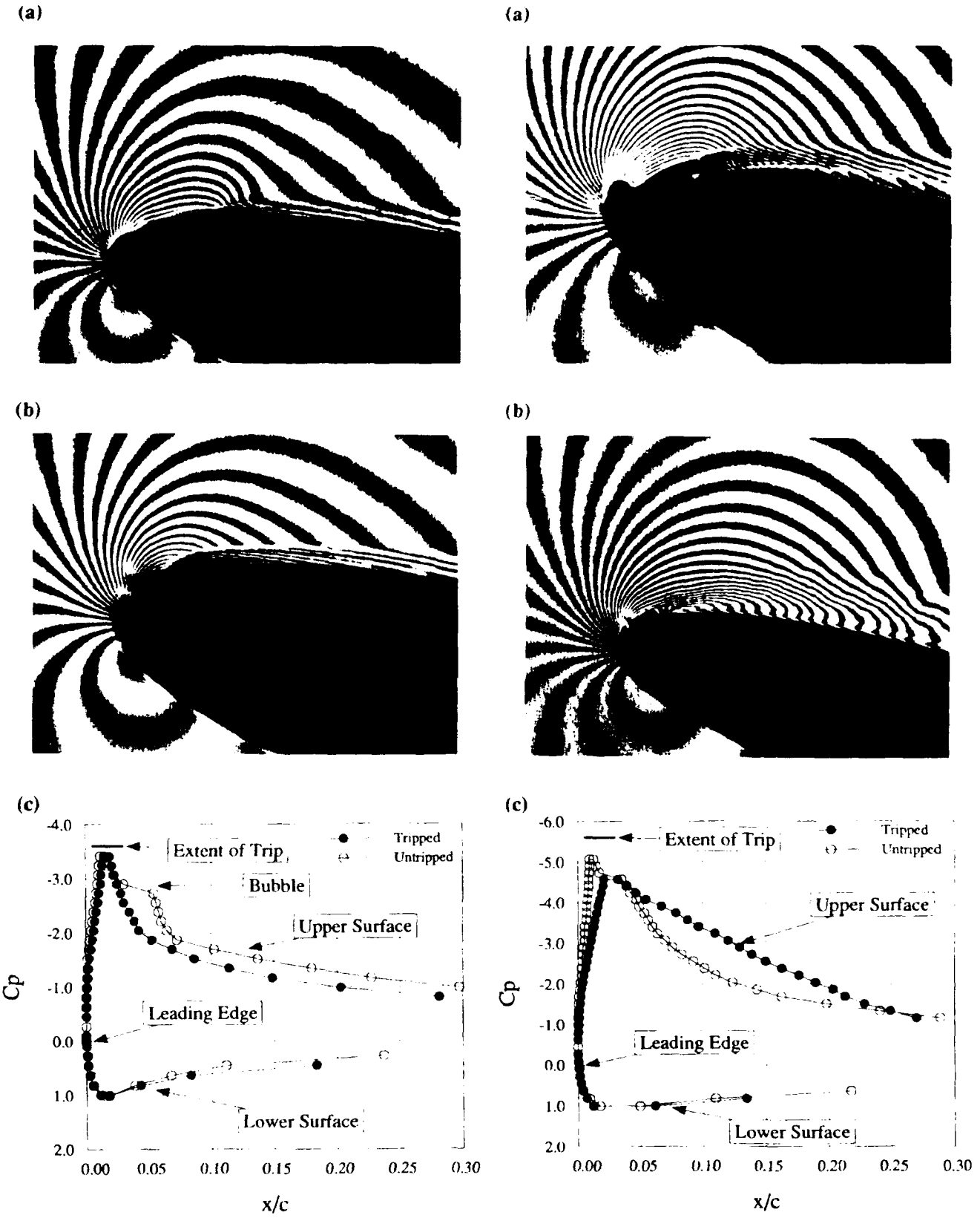

Figure 2. Comparison of Untripped and Tripped Flows, M = 0.3, $\alpha^+ = 0.04$, $\alpha = 11^0$; (a) Untripped Flow Over the First 18% Chord, (b) Tripped Flow Over the First 15% Chord, (c) Pressure Distributions Corresponding to (a) and (b).

Figure 3. Comparison of Untripped and Tripped Flows, M = 0.3, $\alpha^+ = 0.04$, $\alpha = 15^0$; (a) Untripped Flow Over the First 16% Chord, (b) Tripped Flow Over the First 27% Chord, (c) Pressure Distributions Corresponding to (a) and (b).

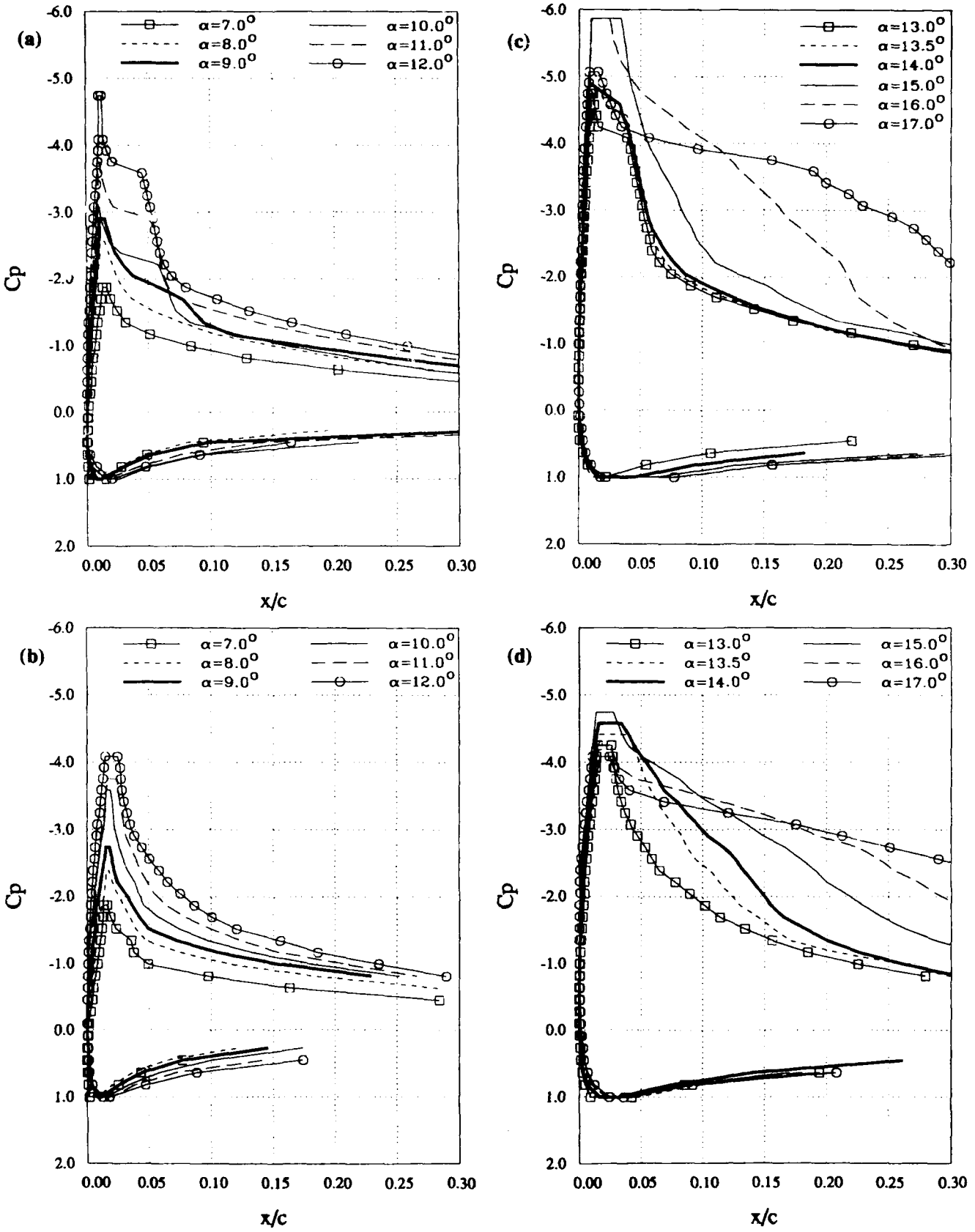

Figure 4. Pressure Distributions over a Transiently Pitching Airfoil, M = 0.3, $\alpha^+ = 0.03$; (a) Untripped, α = 7^0 to 12^0, (b) Tripped, α = 7^0 to 12^0, (c) Untripped, $\alpha = 13^0$ to 17^0, and (d) Tripped, $\alpha = 13^0$ to 17^0

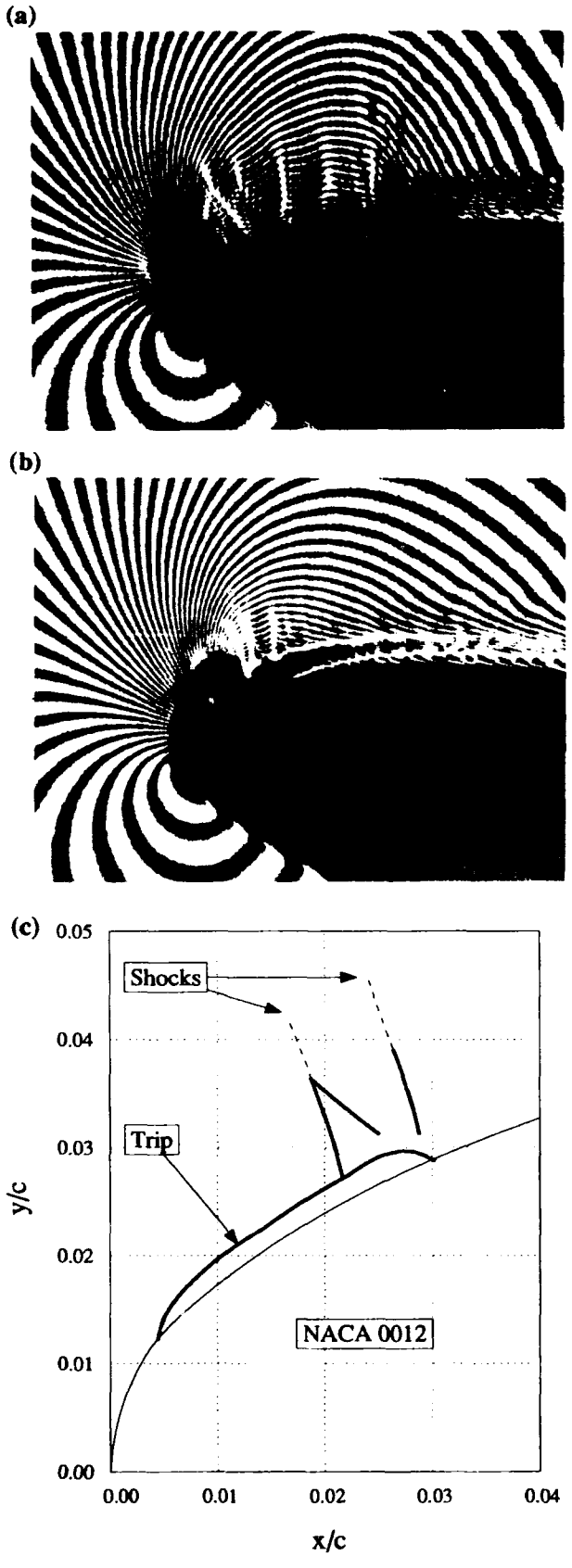

Figure 5. Comparison of Tripped and Untripped Flows Over the First 15% Chord, M = 0.45, $\alpha^+ = 0.025$, $\alpha = 11^0$; (a) Untripped Flow, (b) Tripped Flow, (c) Shock Location Relative to the Trip, Corresponding to Fig. (b).

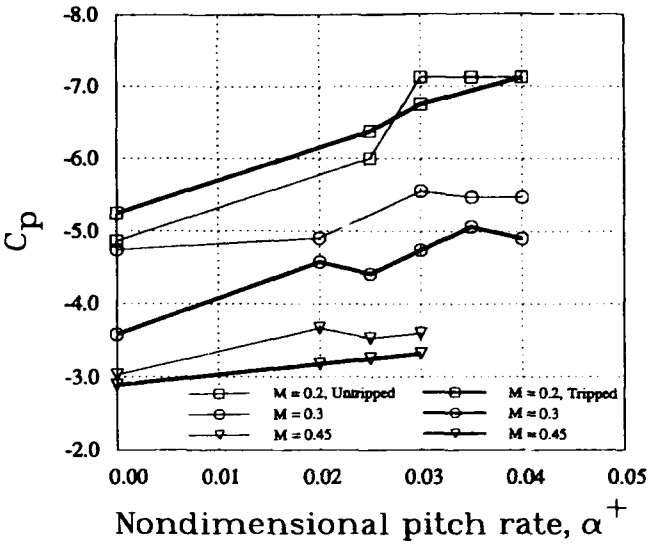

Figure 6. Transiently Pitching Airfoil Peak Suction Pressure Coefficient at Stall Vortex Formation.

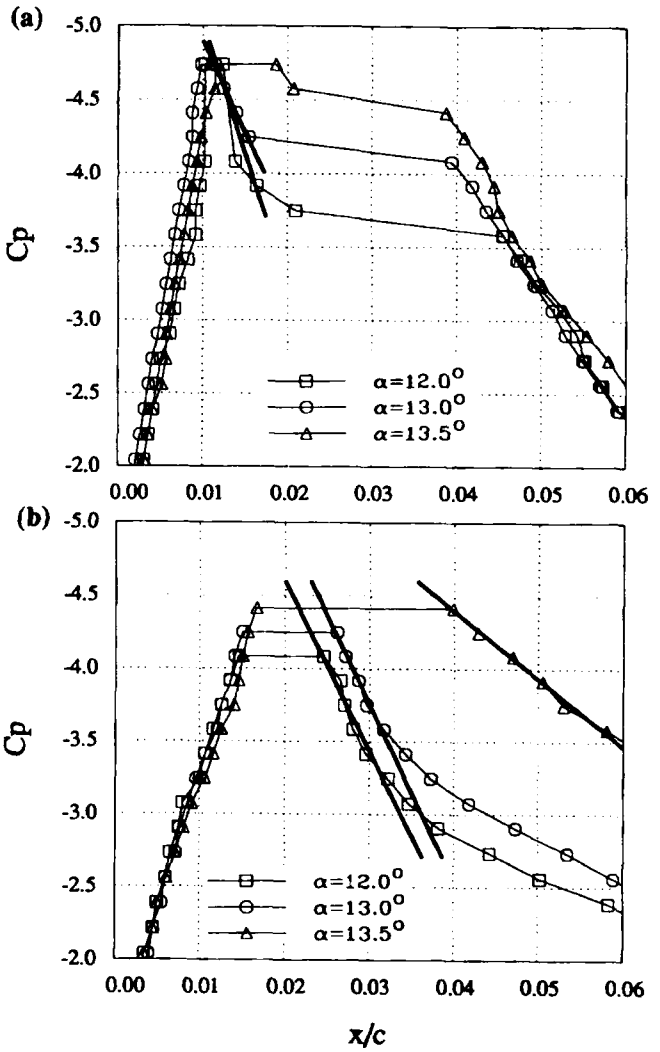

Figure 7. Leading Edge Suction Pressure Distributions, M = 0.3, $\alpha^+ = 0.03$. Slope of Solid Lines Indicates Magnitude of Adverse Pressure Gradient; (a) Untripped, (b) Tripped.

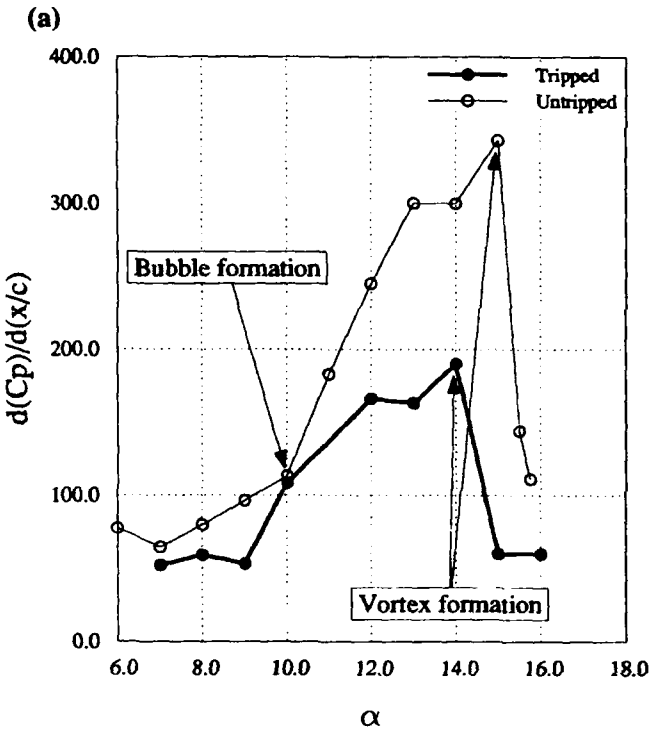

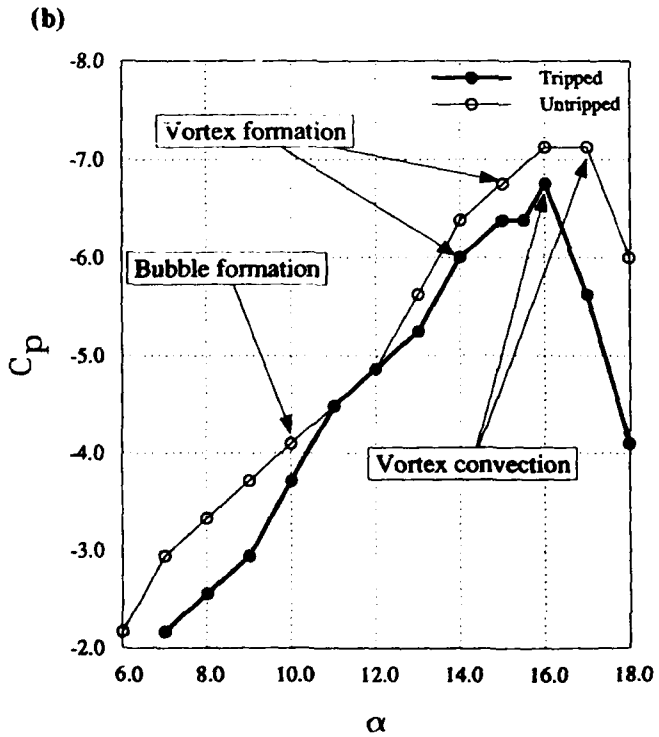

Figure 8. (a) The Development of the Leading-Edge Adverse Pressure Gradient; (b) The Development of the Peak Pressure Coefficient, M = 0.2, $\alpha^+ = 0.03$.

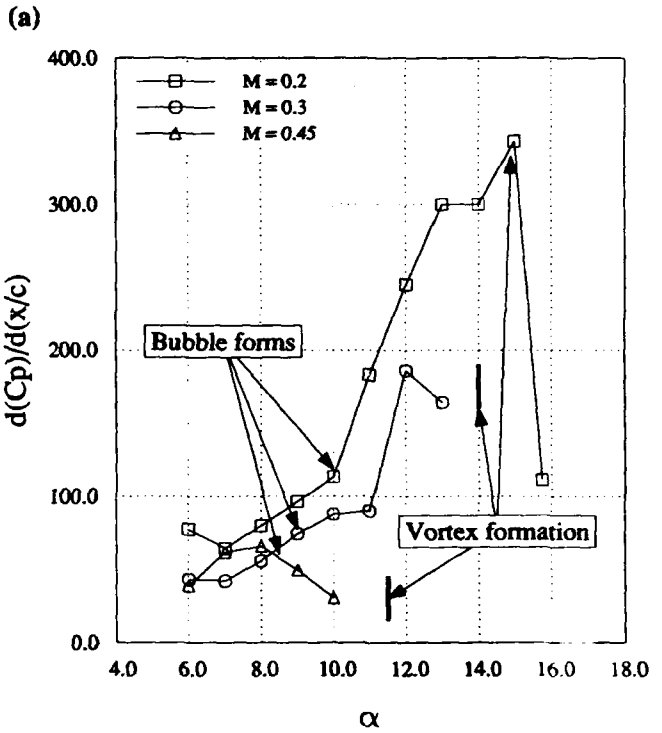

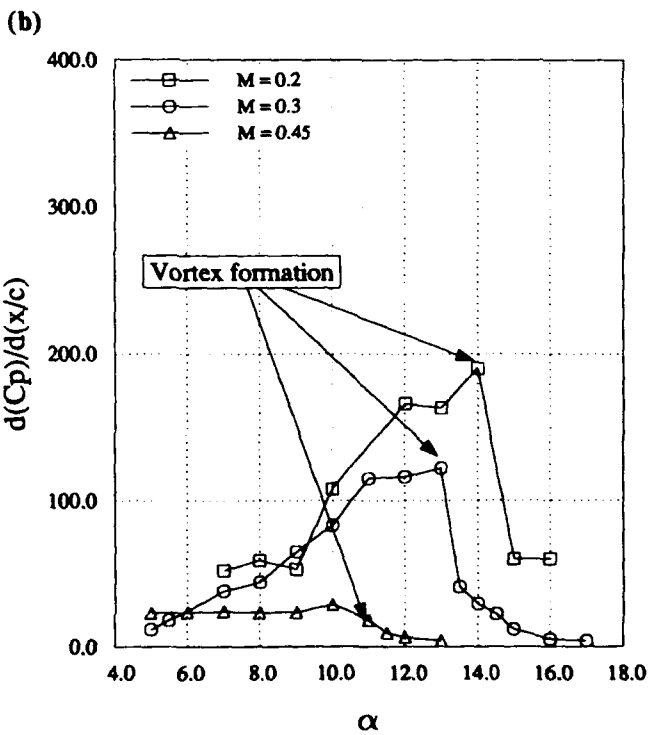

Figure 9. Effect of Mach Number on the Adverse Pressure Gradient Development, $\alpha^+ = 0.03$; (a) Untripped Flow, (b) Tripped Flow.

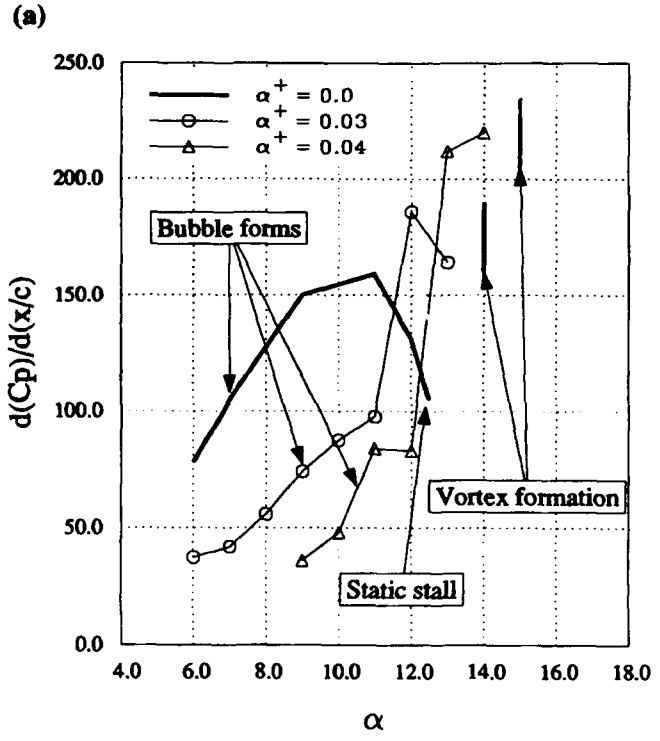

Figure 10. Effect of Pitch Rate on the Adverse Pressure Gradient Development, M =0.3; (a) Untripped Flow, (b) Tripped Flow.

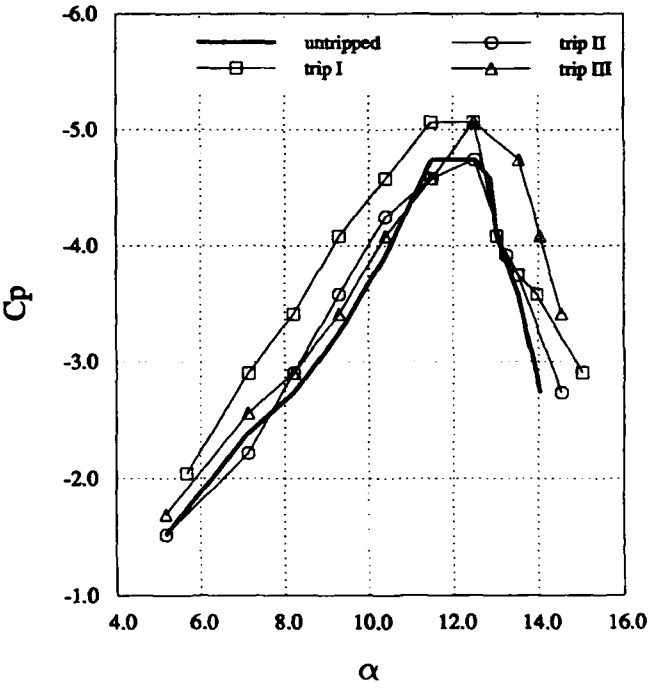

Figure 11. Peak Suction Pressure Coefficient Development over an Oscillating NACA 0012 Airfoil for Various Boundary Layer Trips. M = 0.3, $k = \frac{\pi fc}{U_\infty}$, $\alpha = 10^0 + 10^0 sin\ 2\pi ft$.